ACS SyntheticBiology

pubs.acs.org/synthbio

Research Article

A Synthetic Genetic Circuit Enables Precise Quantification of Direct Repeat Deletion in Bacteria

Yajia Huang, Shuai Yang, Wenhui Chen, Feixuan Li, Aiguo Xia, Lei Ni,* Guang Yang,* and Fan Jin*

Cite This: *ACS Synth. Biol.* 2020, 9, 1041−1050

Read Online

ACCESS | Metrics & More | Article Recommendations | Supporting Information

ABSTRACT: Quantification of the rate of direct repeat deletion (DRD) is an important aspect in the research of DNA rearrangement. The widely used tetracycline selection method usually introduces antibiotic pressure to the tested organism, which may interfere with the DRD process. Also the length of repeat arm (LRA) is limited by the length of the TetR coding sequence. On the basis of the fluorescent microscopy and high-throughput imaging processing, here we developed a two-module genetic circuit, termed TFDEC (which stands for three-color fluorescence-based deletion event counter), to quantify the DRD rate under neutral conditions. DRD events were determined from the state of a three-state fluorescent logic gate constructed through coupling of an OR gate and an AND gate. TFDEC was applied in *Pseudomonas aeruginosa*, and we found that the DRD rate was RecA-dependent for long repeat arms (>500 bp) and RecA-independent for short repeat arms (<500 bp), which was consistent with the case in *Escherichia coli*. In addition, the increase of DRD rate followed an S-shaped curve with the increase of LRA, while treating cells with ciprofloxacin did not change the LRA-dependence of DRD. We also detected a significant increased DRD rate for long repeat arms in the *uvrD* (8-fold) and *radA* (4-fold) mutants. Our results show that the TFDEC method could be used as a complement tool for quantification of the DRD rate in the future.

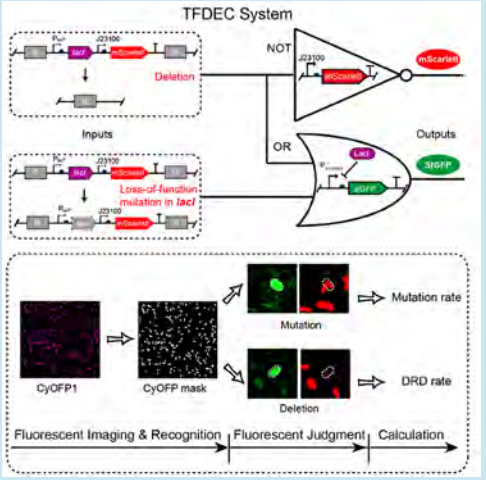

KEYWORDS: *direct repeat deletion, three-color fluorescence-based logic gate, Pseudomonas aeruginosa, synthetic genetic circuit, TFDEC system*

Repeat sequences are ubiquitous in the genome of prokaryotes and eukaryotes.[1,2] Rearrangement between direct repeat sequences can result in deletions or expansions of DNA sequences, which is an important source of genetic plasticity and is involved in the regulation of transcription and protein coding sequence variation.[3−6] Previous studies have suggested that replication fork stalling, which frequently triggers replication fork repair processes, is the main inducement of DNA rearrangement.[7,8] The possible mechanisms of direct repeat deletion (DRD) have been extensively characterized in *Escherichia coli*, including the RecA-dependent recombination and RecA-independent pathways such as replication slippage, sister-chromosome exchange (SCE), and single-strand annealing.[9−13] However, detailed processes of genetic rearrangement under various conditions is far from clear.

Quantification of a genetic rearrangement rate is one primary aspect in deciphering its underlying mechanisms. Previously, the popular antibiotic resistance selection method, commonly achieved by inserting direct repeats within the coding sequence of *tetR*, has been successfully used to quantify the DRD rate.[9,10,13] However, this method often bears the interference of false positive colonies, and the antibiotics used to isolate target transformants may affect the physiological process of genetic rearrangement in host organisms. In addition, the length of the repeat arm (LRA) could not be larger than the length of TetR coding sequence, which would limit the quantification of DRD for long repeats. Therefore, it is beneficial to explore complement techniques to the antibiotic resistance selection method.

The burgeoning field of synthetic biology allows biologists to solve problems with synthetic genetic circuits, the genetic logic gates of which are frequently used to integrate cellular signals.[14,15] Cascading and layering modular genetic logic gates confer engineered organisms the capability of implementing sophisticated functionalities, as exemplified by the toggle switch, synchronized oscillator, and counter.[16−20] These studies inspired us to construct a reporter of DRD using existing genetic tools. Previously, foreign DNA was successfully introduced into the chromosome through single-crossover of

Received: June 17, 2019
Published: April 16, 2020

https://dx.doi.org/10.1021/acssynbio.9b00256
ACS Synth. Biol. 2020, 9, 1041−1050

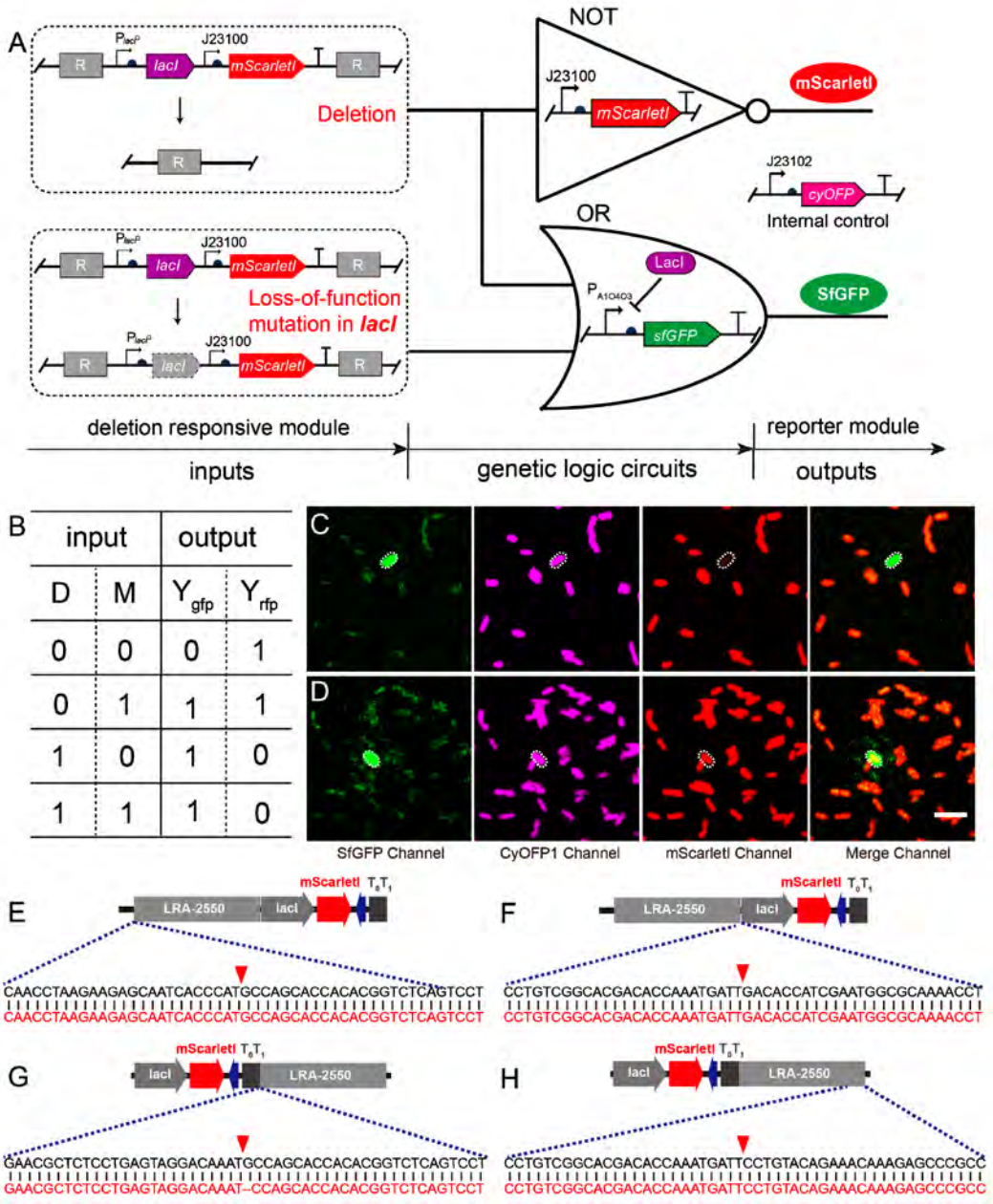

Figure 1. Schematic of the NOT and OR Genetic Gate Design in TFDEC System. (A) Schematic of gene circuit of TFDEC system, comprising the deletion responsive module and the fluorescent reporter module. The deletion and mutation events act as the inputs. The transcription of the output P_{A1O4O3} promoter is turned on when *lacI* is deleted through repeat deletion or inactivated through mutation, while the expression of *mScarletI* is turned off when repeat (*mScarletI*) is deleted. (B) The truth table of TFDEC system. (C) Cell with deletion between repeats (circled with dotted line) that exhibits a high level of SfGFP expression and low level of mScarletI expression. (D) Cell with loss-of-function mutation in *lacI* (circled with dotted line) that exhibits high level of SfGFP expression and high level of mScarletI expression. The DNA fragments (E,F, fragment, left; and G,H, fragment, right) from the joints between different genetic structures were cloned and sequenced, in which the black letters "ATCG" represent the original sequences, while the red letters "ATCG" represent the sequencing results. Scale bar in panel D is 2 μm.

an identical fragment between introduced DNA and the chromosome, resulting in a tandem duplication of the homologous fragment.[21] This tandem repeat sequences have a chance to perform a second crossover and again delete the DNA in between. Thus, a genetic module inserted between direct repeats as an output will constitute a NOT gate together with DRD events as an input. However, mutations occurred in the output module can bring false positive results, thus separating DRD from mutation events is necessary.

Taking advantage of this knowledge, in this study, we designed a two-module genetic circuit, termed three-color fluorescence-based deletion events counter (TFDEC), to quantify the DRD rate. A *lacI* expression module inserted between repeat arms together with a P_{A1O4O3}-*sfgfp* reporter module constitutes an OR gate in response to *lacI* loss-of-function mutations or DRD. An *mScarletI* expression module following *lacI* acts as a NOT gate in response to DRD events. This system distinguishes DRD events from *lacI* loss-of-function mutation by exhibiting different on/off states in

https://dx.doi.org/10.1021/acssynbio.9b00256
ACS Synth. Biol. 2020, 9, 1041−1050

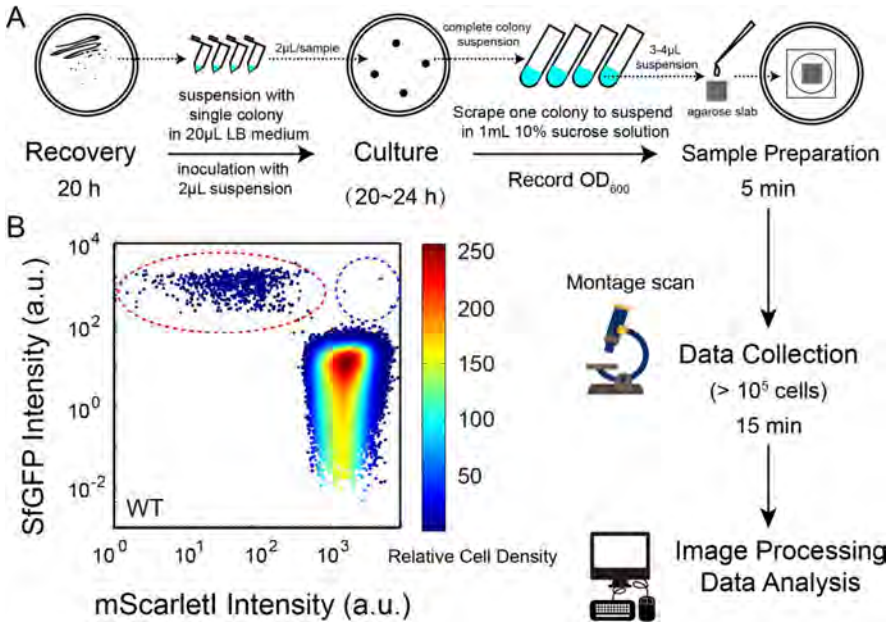

Figure 2. Procedure diagram and statistical analysis of DRD rate. (A) Bacterial strains were recovered and cultured on LB agar plates, and resuspended in 10% (*w*/*v*) sucrose solution before acquisition of fluorescent images. More than 400 image-fields were scanned, and over 10^5 cells were recorded for each sample. Then image processing and data analysis were done in the context of MATLAB. The whole procedure took less than 45 h. (B) SfGFP intensity was plotted against the mScarletI intensity for all recorded single cells of wild type in a 2-D graph, where cells with high expression of SfGFP and low expression of mScarletI were determined to be deletion cells (circled with a red dotted line), while cells with a high expression of SfGFP and a high expression of mScarletI were determined to be *lacI* loss-of-function mutation cells (circled with a blue dotted line). The color map to the right of the panel indicates the relative cell density.

SfGFP/mScarletI expression. By combining fluorescent microscopy and high-throughput imaging processing, the DRD rate can be estimated through statistical analysis of single-cell fluorescence. It is easy to operate for the TFDEC system and convenient for quantification of the DRD rate under various conditions. We have characterized the LRA-dependence of the DRD rate, with or without the treatment of ciprofloxacin, and investigated the role of RecA in DRD. We also quantified the effects of chromosomal positions, spacer lengths between repeats arms (SLRA), and inactivation of multiple recombination-related genes on the DRD rate in *P. aeruginosa*.

RESULTS

Establishment of the TFDEC System Based on a Combination of Genetic NOT Gate and OR Gate. In our proposed method, two genetic modules, namely a deletion responsive module and a reporter module, were incorporated into the chromosome of *P. aeruginosa* (Figure 1A, Figure S1). The deletion responsive module encoded a suppressor (lactose repressor, LacI) and a red fluorescent protein (mScarletI), flanked by two direct repeat sequences. This module was integrated into the chromosome based on a single-crossover method (Figure S1A),[21] and the site of integration could be adjusted using different homologous sequences. The reporter module encoded two fluorescent proteins, namely a green fluorescent protein (SfGFP) expressed by a LacI repressible promoter (P_{A1O4O3}) and an orange fluorescent protein (CyOFP1) expressed by a constitutive promoter (J23102) (Figure S1B). Constitutively expressed CyOFP1 provides a standard protocol for cell identification in imaging processing. The reporter module was cloned into a fixed chromosomal site using the mini-Tn7 system.[22]

In the original stage, the transcription of P_{A1O4O3} was repressed by LacI, resulting in low expression of SfGFP. Meanwhile, mScarletI was expressed normally; thus, the TFDEC system was in an off−on−on state for green (SfGFP), red (mScarletI), and orange (CyOFP1) fluorescence. When DRD events occurred with the deletion of *lacI*, *mScarlet*, and one of the repeat arms, the repression of P_{A1O4O3} would be removed, and the expression of mScarletI would be lost, which converted the TFDEC system to be at the on−off−on state (Figure 1C). However, when loss-of-function mutations occurred in *lacI*, both the green and red fluorescent proteins would be expressed, thus the TFDEC system would be switched to be at the on−on−on state (Figure 1D). Notably, because the frequency for loss-of-function mutation in *lacI* and DRD events occurring simultaneously in one cell was negligible, we assigned the cells with a high level of SfGFP expression and low level of mScarletI expression as the DRD events. The genetic logic gates and truth table were indicated in Figure 1A and Figure 1B, respectively. Also, the DNA fragments cloned from deletion responsive module were confirmed by sequencing before the DRD events occurred (Figure 1E−1H, Figures S2 and S3) and after the DRD events occurred (Figure S4). We also quantified the pseudopositive DRD rate coming from the fluorescent protein expression noise in a control strain (with SfGFP expressed by an inhibited P_{A1O4O3} promoter and mScarletI expressed constitutively, but without direct repeats), in which the pseudopositive effect is marginal (Figure S5).

Procedures for the Quantification of the DRD Rate Using the TFDEC System. The complete procedure for quantification of the DRD rate involved several steps (Figure 2A):

https://dx.doi.org/10.1021/acssynbio.9b00256
ACS Synth. Biol. 2020, 9, 1041−1050

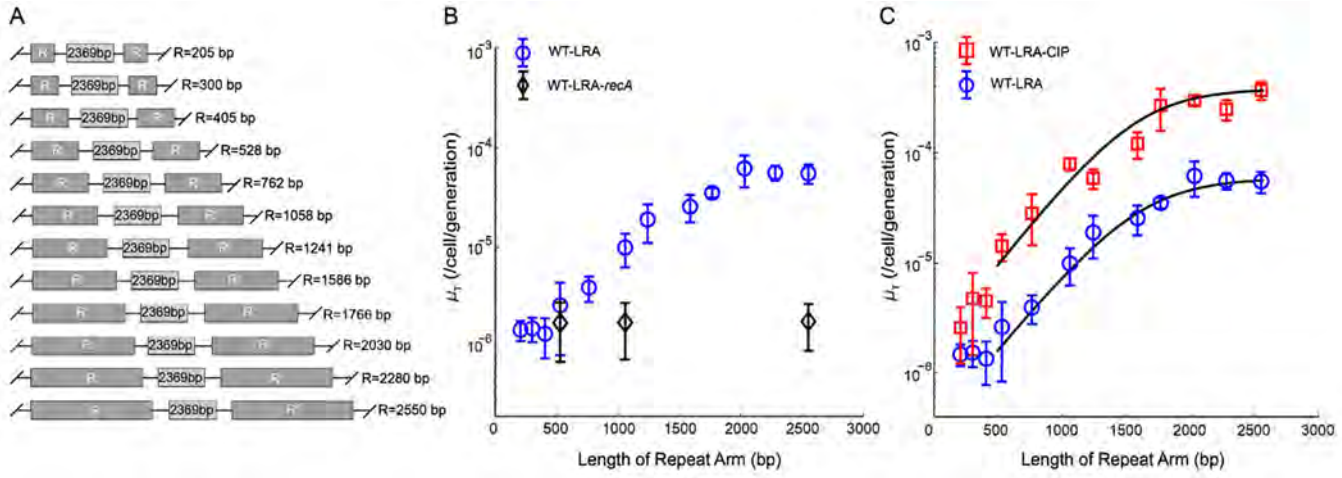

Figure 3. Quantification of the dependence of DRD rate on LRA. (A) Diagram of mutants with different LRAs from 205 to 2550 bp, where the SLRA is fixed to 2369 bp. (B) The DRD rate was plotted as a function of the LRA from 205 to 2550 bp in wild type (marked with blue circles) or in *recA* mutants (marked with black diamonds). (C) The DRD rate was plotted as a function of the LRA from 205 to 2550 bp in wild type (marked with blue circles) and in wild type with treatment of 0.4 μg/mL ciprofloxacin (marked with red squares). The variation trend of DRD rate with the increase of LRA larger than 500 bp was indicated with black solid lines. Here, error bars indicate standard deviation arising from three independent experiments.

(i) Bacteria recovery and incubation. We extended the growth time of bacteria and conducted an expanded culture step by growing large colonies on LB plate, thereby, the resultant large colony was grown from one single cell, during which the DRD events occurred. The average generation number of bacterial growth during colony forming could be easily determined from cell number of the large colony (N_{all}) by $\log_2(N_{all})$. The expanded bacterial culture step enabled us to enrich DRD cells and to harvest enough bacteria for cell counting via OD_{600}. Specifically, scrape one complete colony from the overnight LB plate and thoroughly resuspend it into 20 μL of fresh LB medium. Then inoculate a 2 μL drop of this suspension on an LB plate and incubate for 20−24 h. Further, completely scrape the resultant large colony and resuspend it into 1 mL of fresh 10% (w/v) sucrose solution and record their OD_{600} (1.0−1.2). The generation number (n) of bacteria could be calculated using the following formula: $n = \log_2(10 \times OD_{600} \times 10^9)$, based on the estimation that there were about 10^9 cells in 1 mL of bacterial culture when $OD_{600} = 1$. Bacterial cells dispersed well in 10% (w/v) sucrose solution and thus facilitated the following imaging processing and cell identification in fluorescent images (Figure S6).

(ii) Sample preparation. Pipet 3−4 μL of bacterial suspension onto the top of a 2% (w/v) FAB agarose slab. Let the sample dry for 1 min and flip the agarose slab. Then bacterial cells are sandwiched between the agarose slab and cover glass.

(iii) Acquisition of microscopic images. Fluorescent images of SfGFP, CyOFP1, and mScarletI were snapped subsequently using the montage method[23] to record $>10^5$ single cells from over 400 image-fields for each sample.

(iv) Automatic imaging processing and DRD rate calculation. The frequency of DRD cells could be calculated by using $x = N_{del}/N_{all}$, where N_{del} is the number of deletion cells and N_{all} is the total number of recorded cells. We plotted SfGFP intensities against mScarletI intensities of all recorded single cells, and those with high intensity of SfGFP and low intensity of mScarletI were determined as the DRD cells (Figure 2B, Figure S7). Then the DRD rate (per cell per generation) could be calculated by using $\mu_T \approx x/n$ (see Methods).

The total time duration of this method was less than 45 h, with an operation time of less than 30 min for each sample (Figure 2A). Also, during the culture on LB plates, the cell number in the colony reaches saturation after 27 h of growth, thus cells are able to divide and grow when we harvest them in 20−24 h (Figure S8). Owing to the flexibility of single-crossover used in the deletion responsive module, quantification of DRD rate at any chromosomal site or for different LRAs could be easily achieved through simply altering the sequences of repeat arm. In addition, the TFDEC method enabled us to estimate the rate of mutation and DRD simultaneously, which could hardly be achieved through the antibiotic resistance selection method.

Quantification of the LRA-Dependent DRD Rate. To determine the effect of different LRAs on the DRD rate, we constructed a series of TFDEC strains with LRAs ranging from 205 to 2550 bp (Figure 3A). An S-shaped curve was observed, in which the DRD rate kept a constant low level at LRA less than 500 bp, increased exponentially at LRA from 500 to 1200 bp, and reached plateau at LRA larger than 2000 bp (Figure 3B). By contrast, the DRD rate of *recA* mutants at different LRAs remained unchanged, approximately equal to that of the wild type at an LRA less than 500 bp (Figure 3B). Therefore, DRD in *P. aeruginosa* was RecA-independent in short LRAs, whereas RecA-dependent in LRAs larger than 500 bp, which was consistent with the former studies in *E. coli*.[9,10]

We also quantified the DRD rate of cells under the treatment of 0.4 μg/mL ciprofloxacin, which could induce the SOS response in *P. aeruginosa*.[24] DRD rates of short repeat arm (LRA < 500 bp) and long repeat arm (LRA > 500 bp) were enhanced about 3- and 6-fold by ciprofloxacin treatment, respectively (Figure 3C). However, with the treatment of ciprofloxacin, DRD rate increased similarly with the increase of

https://dx.doi.org/10.1021/acssynbio.9b00256
ACS Synth. Biol. 2020, 9, 1041−1050

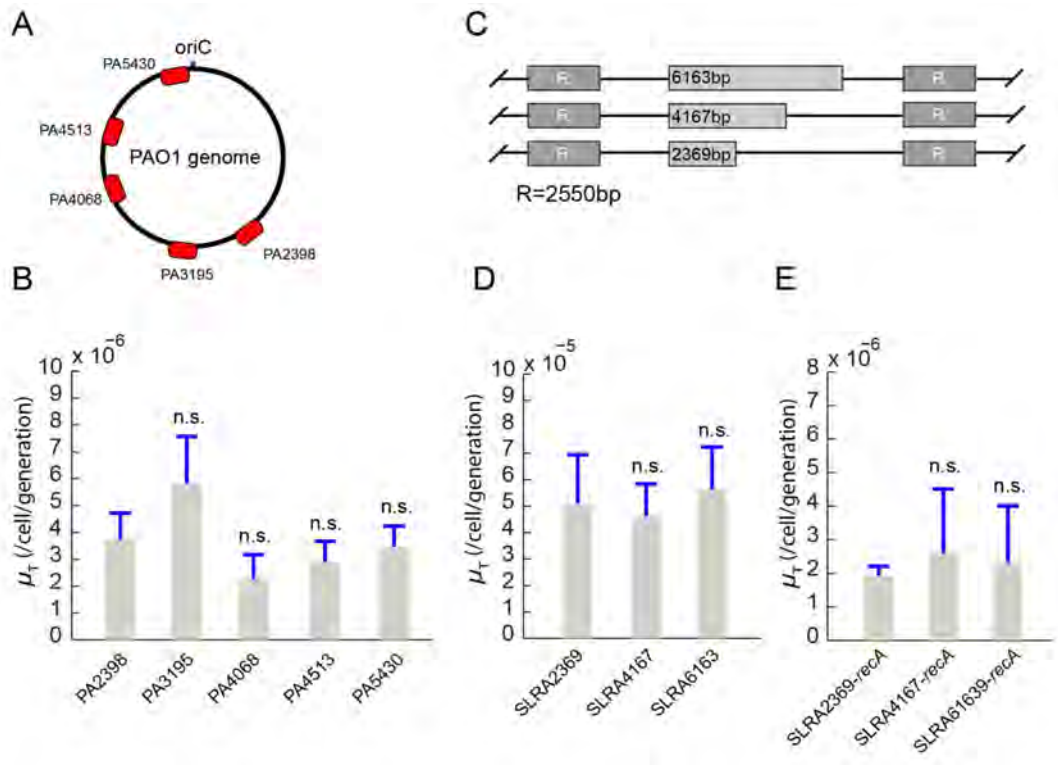

Figure 4. DRD rate is independent of the chromosomal positions and SLRA. (A) A diagram of different sites of direct repeat insertion in the PAO1 chromosome. Here, the LRA is fixed to 2550 bp and SLRA is fixed around 1000 bp (without mScarletI between repeat arms). (B) DRD rate of TFDEC systems with different chromosomal insertion sites (PA2398, PA3195, PA4068, PA4513, and PA5430). Here, the statistical analysis used pairwise comparisons (vs PA2398) (*t* test). (C) Diagram of the mutants with different SLRAs (2369 bp, 4167 bp, and 6163 bp), for which the LRA is fixed to 2550 bp. (D) DRD rate in TFDEC systems with different SLRAs. Here, the statistical analysis used pairwise comparisons (vs SLRA2369) (*t* test). (E) DRD rate in *recA* mutants with different SLRAs. The statistical analysis used pairwise comparisons (vs SLRA2369-*recA*) (*t* test). Here, n.s. represents nonsignificant, and error bars indicate standard deviation from three independent experiments.

LRA (LRA > 500 bp) as compared with the curve without treatment of ciprofloxacin (Figure 3C), indicating that there might be a general mechanism underlying the LRA dependence of DRD. Ciprofloxacin was also applied in two *recA* mutants with different LRAs. Compared with the corresponding value in the same strains without ciprofloxacin treatment, no significant increase of DRD rate was observed in both LRAs (Figure S9).

DRD Rate Was Independent of Chromosomal Sites and SLRA. We further studied the DRD rates at different chromosomal sites or different SLRAs in *P. aeruginosa*. There are reports that double strand breaks occur more in the terminus region of replication,[25] which is opposite to the replication origin site in PAO1,[26] but the precise terminus site is not determined to date. Five strains were constructed by setting the repeats to be the downstream of coding sequence of PA2398, PA3195, PA4068, PA4513, and PA5430 without interfering with the normal expression of these genes, in which PA5430 was near the origin site of replication (Figure 4A). No significant difference of DRD rate was detected between these strains (Figure 4B), as the terminus region was probably missed by us. DRD rates in three different SLRAs (2369, 4167, and 6163 bp) were also determined, where LRA was fixed to 2550 bp (Figure 4C) and no significant difference was observed as well (Figure 4D). This was consistent with a pioneer finding that the RecA-dependent deletion of tandem repeats showed little proximity effect.[27] In addition, according to our experiments, SLRA also showed a marginal effect on the DRD rate in *recA* mutant strains (Figure 4E), which was inconsistent with several previous studies.[12,27] The contradiction might be due to the relatively high noise of our method when the DRD rate was low.

DRD Was Enhanced in *uvrD* and *radA* Mutants. According to the data in Figure 3B, DRD for long repeat arms was RecA-dependent. Regarding that RecA is the key factor in recombination, we next selected several recombination-related genes to inactivate to quantify DRD rates. RecBCD and RecFOR are the two sets of mediator proteins that loads RecA to single-stranded DNA (ssDNA).[28−30] The RecF pathway, with the help of the RecO, RecR, and RecQ helicase and the RecJ exonuclease, mediates ssDNA gap repair through recombination,[30−34] and also repairs DNA double-strand breaks (DSBs) in the *recBrecCsbcBsbcC* mutant background.[35,36] The SbcC-SbcD nuclease complex is essential in processing convergent forks to complete during chromosome replication.[37] RecN is a cohesin-like protein that stimulates DNA strand invasion in RecA-mediated recombination.[38] MutS is a component of DNA mismatch repair machinery that modulates recombination of divergent sequences.[39,40] RadA was proposed to be a DnaB type helicase that facilitates bidirectional D-loop extension in the process of RecA-driven ssDNA recombination.[41] Whereas a recent study found that RadA can unwind forked DNA from 5′ to 3′ that DnaB cannot do.[42] In addition, the UvrD helicase functions in mismatch repair and nucleotide excision repair, and facilitates RecA removal from nucleoprotein filaments during recombination.[43−45] Thus, we quantified DRD rates in those recombination-related knockout strains, for which the LRA and SLRA

https://dx.doi.org/10.1021/acssynbio.9b00256
ACS Synth. Biol. 2020, 9, 1041−1050

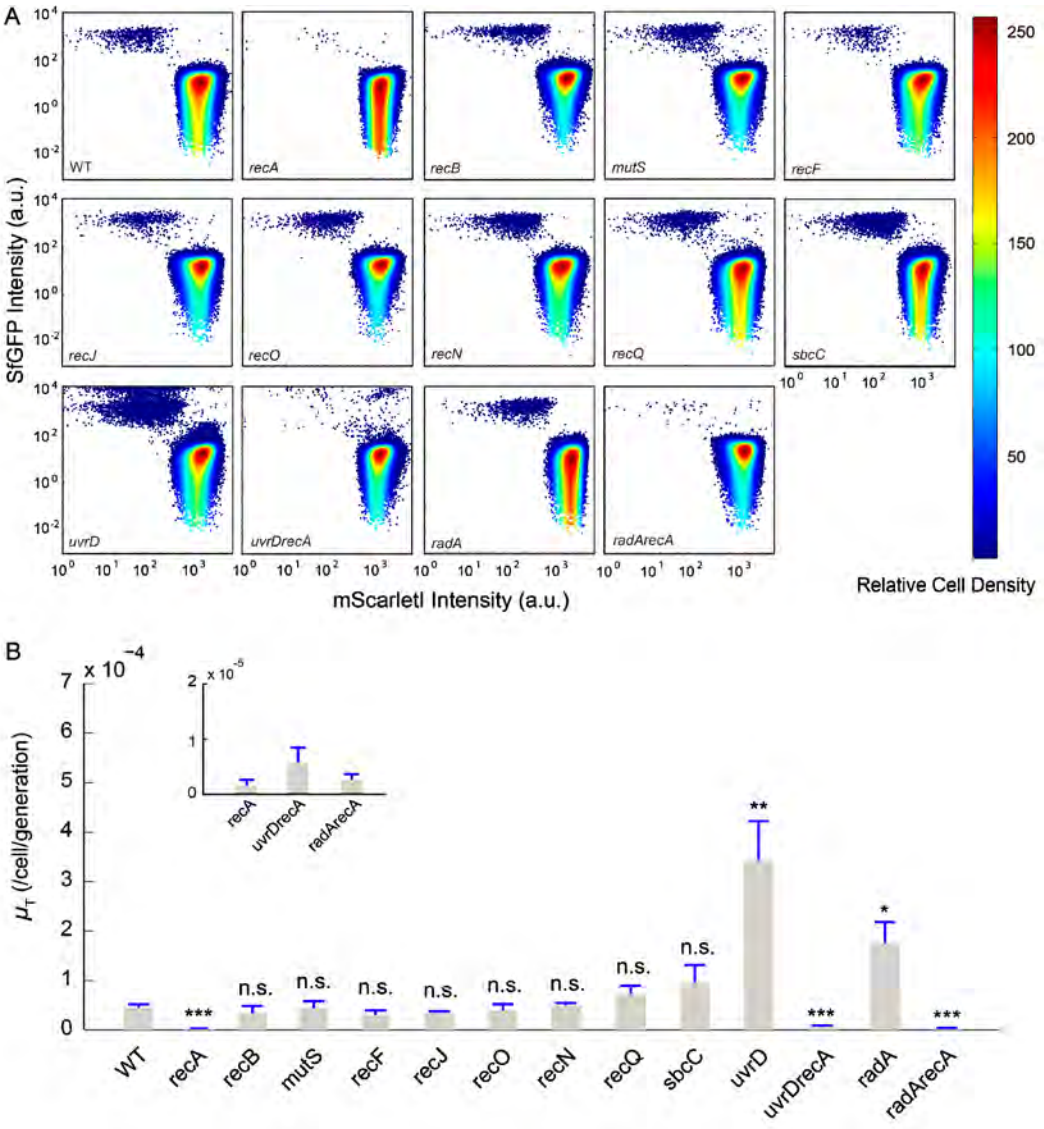

Figure 5. Quantification of DRD rate in various recombination-related mutants of *P. aeruginosa*. (A) SfGFP intensity was plotted against mScarletI intensity from all recorded single cells in each mutant. The color map to the right of the panel indicates the relative cell density. (B) DRD rates in multiple recombination-related mutants. The statistical analysis used pairwise comparisons (vs wild type) (*t* test). Here, ***$P < 0.001$, **$P < 0.01$, *$P < 0.05$, and n.s. represents nonsignificant. In all mutants, the LRA is fixed to 2550 bp, SLRA is fixed to 2369 bp, and error bars indicate standard deviation from three independent experiments.

of TFDEC system in all strains was fixed to 2550 bp and 2369 bp, respectively.

As displayed in Figure 5 and Table S1, DRD rates were not affected in cells devoid of RecB, RecF, RecO, RecJ, RecN, RecQ, MutS, and SbcC ($P > 0.05$), which made the exact mechanism of how RecA contributed to DRD in *Pseudomonas aeruginosa* uncertain. Moreover, in the *uvrD* mutant, the DRD rate was approximately 8-fold ($P < 0.01$) higher than that in the wild type, which was consistent with previous results in *D. radiodurans* and *E. coli*.[13,46] This might result from the antagonism effect that UvrD dismantles the RecA-ssDNA filaments, or the reduced fidelity of DNA replication and induced SOS response in bacteria after UvrD inactivation.[46,47] Unexpectedly, the DRD rate in *radA* mutant was approximately 4-fold ($P < 0.05$) higher than that in the wild type, indicating a negative effect of RadA on DRD that remained to be elucidated. Furthermore, DRD rates of *radArecA* and *uvrDrecA* mutants dropped to the level of *recA* mutant, suggesting that the antagonism activities of RadA and UvrD to DRD were both mediated by some RecA-dependent pathways.

TFDEC Enables the Quantification of DRD and Mutation Rate Simultaneously. To examine the relationship between DRD and mutation, we plotted the loss-of-function mutation rates in *lacI* against the DRD rate of all the tested mutants in one map, where each data point was colored according to its relative fitness (normalized by the fitness of wild type). As displayed in Figure 6, a moderate positive correlation (correlation coefficient (cc) = 0.55) was observed between the DRD rate and mutation rate among *recA*$^+$ mutants, while a higher positive correlation (cc = 0.97) was observed in the six *recA*$^-$ mutants (*uvrDrecA*, *recFrecA*, *radArecA*, *sbcCrecA*, *recOrecA*, and *recA*). The DRD rate in wild-type bacteria reflects the frequency of replication fork stalling, which frequently resulted from the DNA lesions or single-strand DNA breaks.[7,8] This might be why strains with higher mutation rates (with larger frequency of DNA damage)

https://dx.doi.org/10.1021/acssynbio.9b00256
ACS Synth. Biol. 2020, 9, 1041−1050

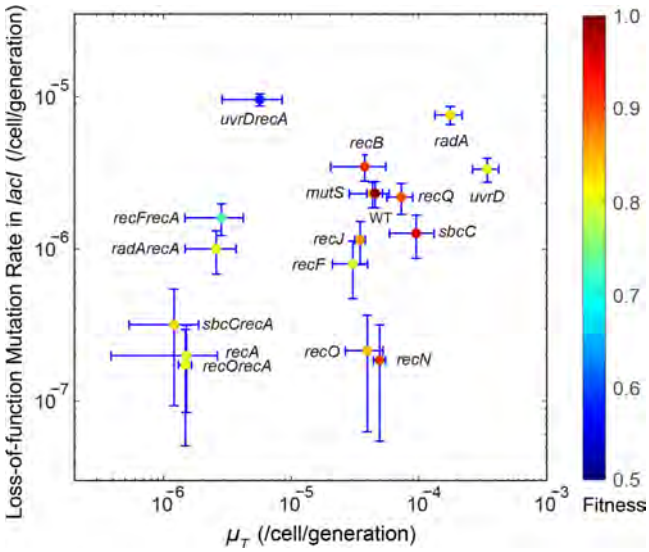

Figure 6. DRD rate was plotted against *lacI* loss-of-function mutation rate. The *lacI* loss-of-function mutation rates of various recombination-related mutants were plotted against their DRD rates. Each data point was colored according to its relative fitness (normalized by the fitness of wild type). Here, in all mutants, the LRA is fixed to 2550 bp and SLRA is fixed to 2369 bp.

tend to have higher DRD rates. Besides, the fitness of *recA*$^-$ mutants are 20−40% less than that of *recA*$^+$ strains, consistent with the fact that RecA facilitates DSB repair and replication fork repair in bacteria.[48,49]

It is worth noting that our results of *lacI* loss-of-function mutation rate failed to repeat previous reported increased mutation frequency of *mutS* mutant in *E. coli* and other organisms. We also tested the mutation frequency of *Pseudomonas aeruginosa* using rifampicin selection, the result in *mutS* mutant was 500-fold higher than that in wild type (Figure S10). This inconsistency was probably due to the different mechanism of mutation detection between *lacI* loss-of-function and rifampicin selection. Acquisition of rifampicin resistance requires proper mutations at specific sites in *rpoB*, thus rifampicin selection is good to estimate spontaneous, nonframeshift, and base-to-base mutations in bacteria. However, it may miss other kinds of mutations (such as insertions, deletions), which also occur frequently in bacteria. On the other hand, all these mutations (mutation/deletion/insertion) can be reflected through detection of LacI inactivation in bacteria.

DISCUSSION

In this study, we set up a TFDEC system for quantification of DRD rate through the determination of a three-state fluorescence gate in single cells. Due to the low frequency of single crossover recombination under LRA less than 200 bp, it is difficult to construct TFDEC systems for quantification of DRD in shorter repeat arms. Meanwhile, since DRD events resulting from unequal SCE will generate a dimeric chromosome (with repeat number of 1 and 3) in a cell that reserves LacI expression, these DRD events cannot be detected by TFDEC.[11] Nonetheless, compared with the traditional antibiotic resistance selection method, the TFDEC method is devoid of antibiotic selection pressure and enables the quantification of repeat deletion for long repeats and at different chromosomal sites. Besides, the single-crossover and miniTn7 gene-insertion techniques used in TFDEC construction could be easily applied in other bacteria. Therefore, the TFDEC system is a good complement tool to the traditional antibiotic resistance selection method for quantification of the DRD rate.

The CyOFP1 expression from the reporter part of TFDEC is used for cell recognition during image processing. Meanwhile, it can also act as an identification signal for the specified bacteria strains. By replacing CyOFP1 with other kinds of fluorescent proteins, simultaneous quantification of the DRD rate of multiple strains in a mixture of bacteria is achievable. Therefore, TFDEC is a candidate tool for the investigation of DRD in bacterial cells under conditions of multispecies competition or symbiosis.

DRD could be induced externally by DNA damaging agents such as ionizing radiation (IR) or internally by DNA replication problems,[47] thus the DRD rate of bacteria originating from different environments can vary largely. However, in a fixed environment, the DRD rate in one bacteria should be stable and constant with time. Therefore, our TFDEC could be used as a timer by monitoring the frequency of DRD, through a formula $t = x \cdot t_d/\mu$, where t is the total time of the bacteria in a target environment, x is the frequency of repeat deletion, t_d is the doubling time of bacteria, and μ is the DRD rate. This is especially useful to evaluate growth of bacteria in the gut or other parts of the host which is unachievable by using conventional methods. The timer property of the TFDEC system may also be applied to study the competition of different microorganisms within a host.

In addition, the TFDEC system also serves as a genetic tool that enables SfGFP expression in very few cells among a large population. By replacing SfGFP with other functional proteins and adjusting the LRA in the responsive module, we can generate a small fraction of cells with specific phenotypes and with specified frequencies of occurrence in a bacterial community. This may be useful in the investigation of a persister emergence during antibiotic treatment and in unravelling the roles of certain proteins during stress-driven evolutions of bacterial population.

METHODS

Bacterial Strains and Growth Conditions. Bacterial strains and plasmids used in this study are listed in Table S2. Details for constructions of the gene knockout mutants and growth curve measurement are given in the Supplementary Methods.

Validation of DRD Cells. The strains were grown on LB agar plates at 37 °C for overnight. Monoclonal colonies were inoculated and cultured with fresh LB plates at 37 °C for 20 h. Then the bacterial cultures were gradually further diluted (1:1000) in fresh LB mediums to culture for over 30 cycles. To enable the accumulation of DRD cells, we selected pure colonies in the on−off−on state and amplified the DNA segment of deletion responsive module via the polymerase chain reaction and further confirmed DRD occurrence via sequencing (Figures S2 and S4).

Acquisition of Fluorescent Images by Using Microscope. The samples for microscopic imaging were prepared according to a previously described procedure.[23] In brief, 3−4 μL of bacterial suspension was pipetted out and loaded onto a 1 cm^2 slab made of 2% (w/v) FAB agarose. The bacterial culture dried in 1−2 min through evaporation and absorption. Then the agarose pad was flipped onto a cover glass. In this

https://dx.doi.org/10.1021/acssynbio.9b00256
ACS Synth. Biol. 2020, 9, 1041−1050

way, bacterial cells were sandwiched between the agarose slab and the cover glass. A spinning-disk confocal microscope (Revolution Andor) equipped with a 100× oil objective and an EMCCD camera (iXon 897i Andor) was used to continuously record the fluorescence-labeled bacteria spread over 400 image-fields, where over 10^5 cells were imaged in each sample. For *recA* mutants whose DRD rates are significantly less than 10^{-5} /cell/generation, the recorded number was increased to more than 3×10^5 to reduce the stochastic noise. The SfGFP, CyOFP1, or mScarletI were excited using 488, 488, or 561 nm laser, respectively, and imaged with three emission channels (524, 607, or 607 nm).

Imaging Processing and Data Analysis. The 14 bit fluorescent images of SfGFP, CyOFP1, and mScarlet1 were analyzed using a homemade algorithm coded by MATLAB. Specifically, cell mask images were determined from CyOFP1 images through two times of Gaussian blur and one time of edge filtering, before cutting off with a threshold intensity. Holes of the resulting binary images were filled using the MATLAB's "imfill" function.

To determine the frequency of DRD or *lacI* loss-of-function mutation in one sample, mask images generated from SfGFP images (in which cells were separately distributed because of the low frequency of DRD and *lacI* loss-of-function mutation) were used to determine the number of cells with high level of SfGFP expression. Then, the number of repeat deletion cells (N_{del}) or *lacI* loss-of-function mutation cells (N_m) were determined according to the mScarletI intensity in corresponding SfGFP-expressed cells. The total cell number in the CyOFP1 images (N_{all}) was estimated by $N_{all} \approx A_{all}/A_{mean,cell}$, in which A_{all} was the total area occupied by all bacterial cells in the mask image, $A_{mean,cell}$ was the mean area occupied by a single cell. The frequency of the DRD cells and *lacI* loss-of-function mutation cells was calculated by N_{del}/N_{all} or N_m/N_{all}.

For the drawing of the 2-D single-cell fluorescence graphs shown in Figure 2B or Figure 5A, large cell clusters from CyOFP1 mask images in which single cells were hardly resolved (Figure S6B) were skipped (according to the occupied area in the mask image). The resulting mask images were mapped to the corresponding SfGFP and mScarletI images, respectively, single cell intensities of SfGFP and mScarletI were extracted using the MATLAB's "regionprops" function. Data points from three parallel experiments were combined to generate one 2-D graph.

The fluorescence crosstalks between SfGFP, CyOFP1, and mScarletI were corrected through separate imaging of the purified fluorescent proteins.

More information for the determination of the threshold mScarletI intensity is included in the Supplementary Methods.

Calculation for DRD Rate and *lacI* Loss-of-Function Mutation Rate. The DRD rate was quantified through modification of a previously described method.[50] We assumed that the dynamics of the DRD cells in the population followed the differential equation as below,

$$\frac{dx}{dt} = f_1 x + \mu(1 - x) - \varphi x \tag{1}$$

where x is the frequency of DRD cells, $(1 - x)$ is the frequency of non-DRD cells. f_1 or f_2 represents the fitness of deletion or nondeletion cells, μ is the DRD rate, and $\varphi = f_1 x + f_2(1 - x)$ is the average fitness of the entire population. And $f_1 x - \varphi x$ is the frequency change of DRD cells caused by the difference of growth rate between deletion cells and non-DRD cells, $\mu(1 - x)$ is the frequency increase of DRD cells due to the transformation of non-DRD cells to DRD cells. The solution of eq 1 with the initial condition $x(t = 0) = 0$ (according to the fact that we grew the large colonies from one single nondeletion cell) is

$$x(t) = \frac{\mu}{f_1 - \varphi - \mu}(e^{(f_1 - \varphi - \mu)t} - 1) \tag{2}$$

At the condition $f_1 = f_2$, the solution of $x(t)$ can be further simplified to $x(t) = 1 - e^{-\mu t}$. In the limited condition of $\mu t \ll 1$, one can estimate that

$$x(t) \approx \mu t \tag{3}$$

According to previous study by Bzymek et al.,[11] occurrence of repeat deletion is strongly dependent on DNA replication. Thus, DRD rate is constant when normalized with generation number, rather than with growth time. Equation 3 is applicable when the bacterial growth rate is constant. In most cases in which bacterial growth rate changes with the culture time, the formula could be written as $x(n) \approx \mu_T \cdot n$, where n is the average doubling generations that can be estimated by counting the total populations of bacteria, x can be directly obtained by the number ratio of deletion cells to total recorded cells. The nonsignificant DRD rates were obtained for *P. aeruginosa* under different growth conditions with varied bacterial growth rates (Figure S11), indicating it is reasonable to normalize DRD frequency with generation number.

Also, the *lacI* loss-of-function mutation rate was estimated in a similar way as the DRD rate calculation: $x_m(n) \approx \mu_m \cdot n$, where x_m is the frequency of mutation events and μ_m is the rate of *lacI* loss-of-function mutation.

■ ASSOCIATED CONTENT

Supporting Information

The Supporting Information is available free of charge at https://pubs.acs.org/doi/10.1021/acssynbio.9b00256.

Additional methods, bacterial strains, and growth conditions, cut-off threshold, growth curve measurement; mutations frequency; additional tables and figures (PDF)

■ AUTHOR INFORMATION

Corresponding Authors

Fan Jin − *Institute of Synthetic Biology, Shenzhen Institutes of Advanced Technology, Chinese Academy of Sciences; Shenzhen Institute of Synthetic Biology, Shenzhen Institutes of Advanced Technology, Chinese Academy of Sciences, Shenzhen 518055, P. R. China; Hefei National Laboratory for Physical Sciences at the Microscale, University of Science and Technology of China, Hefei 230026, P. R. China;* orcid.org/0000-0003-2313-0388; Phone: +86-551-6360-6925; Email: fjinustc@ustc.edu.cn; Fax: +86-551-6360-6743

Guang Yang − *Department of Biomedical Engineering, College of Life Science and Technology, Huazhong University of Science and Technology, Wuhan 430074, P. R. China;* orcid.org/0000-0001-9198-3556; Phone: +86-27-8779-3523; Email: yang_sunny@yahoo.com; Fax: +86-27-8779-2265

Lei Ni − *Institute of Synthetic Biology, Shenzhen Institutes of Advanced Technology, Chinese Academy of Sciences; Shenzhen Institute of Synthetic Biology, Shenzhen Institutes of Advanced Technology, Chinese Academy of Sciences, Shenzhen 518055, P. R. China; Hefei National Laboratory for Physical Sciences at*

https://dx.doi.org/10.1021/acssynbio.9b00256
ACS Synth. Biol. 2020, 9, 1041−1050

the Microscale, University of Science and Technology of China, Hefei 230026, P. R. China; Phone: +86-551-6360-6925; Email: nilei@mail.ustc.edu.cn; Fax: +86-551-6360-6743

Authors

Yajia Huang − *Department of Biomedical Engineering, College of Life Science and Technology, Huazhong University of Science and Technology, Wuhan 430074, P. R. China; Institute of Synthetic Biology, Shenzhen Institutes of Advanced Technology, Chinese Academy of Sciences; Shenzhen Institute of Synthetic Biology, Shenzhen Institutes of Advanced Technology, Chinese Academy of Sciences, Shenzhen 518055, P. R. China*

Shuai Yang − *Institute of Synthetic Biology, Shenzhen Institutes of Advanced Technology, Chinese Academy of Sciences; Shenzhen Institute of Synthetic Biology, Shenzhen Institutes of Advanced Technology, Chinese Academy of Sciences, Shenzhen 518055, P. R. China; Hefei National Laboratory for Physical Sciences at the Microscale, University of Science and Technology of China, Hefei 230026, P. R. China;* orcid.org/0000-0001-8325-4994

Wenhui Chen − *Hefei National Laboratory for Physical Sciences at the Microscale, University of Science and Technology of China, Hefei 230026, P. R. China*

Feixuan Li − *Hefei National Laboratory for Physical Sciences at the Microscale, University of Science and Technology of China, Hefei 230026, P. R. China*

Aiguo Xia − *Institute of Synthetic Biology, Shenzhen Institutes of Advanced Technology, Chinese Academy of Sciences; Shenzhen Institute of Synthetic Biology, Shenzhen Institutes of Advanced Technology, Chinese Academy of Sciences, Shenzhen 518055, P. R. China; Hefei National Laboratory for Physical Sciences at the Microscale, University of Science and Technology of China, Hefei 230026, P. R. China*

Complete contact information is available at: https://pubs.acs.org/10.1021/acssynbio.9b00256

Author Contributions

L.N. and F.J. conceived the project. Y.H., S.Y., W.C., F.L., and A.X. performed the experiments. Y.H., L.N., F.J., and G.Y. contributed jointly to data interpretation and manuscript preparation. All authors reviewed the manuscript.

Notes

The authors declare no competing financial interest.

■ ACKNOWLEDGMENTS

This work was supported by the National Key Research and Development Program of China (2018YFA0902700), the National Natural Science Foundation of China (31700087, 21774117 and 31700745). The Fundamental Research Funds for the Central Universities (WK3450000003) also supported this work, in which Yajia Huang and Guang Yang were supported by the National Natural Science Foundation of China (31270150 and 21774039).

■ REFERENCES

(1) Subramanian, S., Mishra, R. K., and Singh, L. (2003) Genome-wide analysis of microsatellite repeats in humans: their abundance and density in specific genomic regions. *Genome Biol. 4*, R13.

(2) Oliveira, P. H., Prather, K. J., Prazeres, D. M., and Monteiro, G. A. (2010) Analysis of DNA repeats in bacterial plasmids reveals the potential for recurrent instability events. *Appl. Microbiol. Biotechnol. 87*, 2157−2167.

(3) Hannan, A. J. (2018) Tandem repeats mediating genetic plasticity in health and disease. *Nat. Rev. Genet. 19*, 286−298.

(4) Padeken, J., Zeller, P., and Gasser, S. M. (2015) Repeat DNA in genome organization and stability. *Curr. Opin. Genet. Dev. 31*, 12−19.

(5) Puopolo, K. M., Hollingshead, S. K., Carey, V. J., and Madoff, L. C. (2001) Tandem repeat deletion in the alpha C protein of group B streptococcus is recA independent. *Infect. Immun. 69*, 5037−5045.

(6) Vinces, M. D., Legendre, M., Caldara, M., Hagihara, M., and Verstrepen, K. J. (2009) Unstable Tandem Repeats in Promoters Confer Transcriptional Evolvability. *Science 324*, 1213.

(7) Goldfless, S. J., Morag, A. S., Belisle, K. A., Sutera, V. A., Jr., and Lovett, S. T. (2006) DNA repeat rearrangements mediated by DnaK-dependent replication fork repair. *Mol. Cell 21*, 595−604.

(8) Michel, B., Flores, M.-J., Viguera, E., Grompone, G., Seigneur, M., and Bidnenko, V. (2001) Rescue of arrested replication forks by homologous recombination. *Proc. Natl. Acad. Sci. U. S. A. 98*, 8181.

(9) Mazin, A. V., Kuzminov, A. V., Dianov, G. L., and Salganik, R. I. (1991) Mechanisms of deletion formation in Escherichin coli plasmids. *Mol. Gen. Genet. 228*, 209−214.

(10) Dianov, G. L., Kuzminov, A. V., Mazin, A. V., and Salganik, R. I. (1991) Molecular mechanisms of deletion formation in Escherichia coli plasmids. *Mol. Gen. Genet. 228*, 153−159.

(11) Bzymek, M., and Lovett, S. T. (2001) Instability of repetitive DNA sequences: The role of replication in multiple mechanisms. *Proc. Natl. Acad. Sci. U. S. A. 98*, 8319.

(12) Lovett, S. T., Gluckman, T. J., Simon, P. J., Sutera, V. A., and Drapkin, P. T. (1994) Recombination between repeats in Escherichia coli by a recA-independent, proximity-sensitive mechanism. *Mol. Gen. Genet. 245*, 294−300.

(13) Ithurbide, S., Bentchikou, E., Coste, G., Bost, B., Servant, P., and Sommer, S. (2015) Single Strand Annealing Plays a Major Role in RecA-Independent Recombination between Repeated Sequences in the Radioresistant Deinococcus radiodurans Bacterium. *PLoS Genet. 11*, e1005636.

(14) Brophy, J. A., and Voigt, C. A. (2014) Principles of genetic circuit design. *Nat. Methods 11*, 508−520.

(15) Wang, B., and Buck, M. (2012) Customizing cell signaling using engineered genetic logic circuits. *Trends Microbiol. 20*, 376−384.

(16) Anderson, J. C., Clarke, E. J., Arkin, A. P., and Voigt, C. A. (2006) Environmentally controlled invasion of cancer cells by engineered bacteria. *J. Mol. Biol. 355*, 619−627.

(17) Friedland, A. E., Lu, T. K., Wang, X., Shi, D., Church, G., and Collins, J. J. (2009) Synthetic gene networks that count. *Science 324*, 1199−1202.

(18) Gardner, T. S., Cantor, C. R., and Collins, J. J. (2000) Construction of a genetic toggle switch in Escherichia coli. *Nature 403*, 339−342.

(19) Saeidi, N., Wong, C. K., Lo, T. M., Nguyen, H. X., Ling, H., Leong, S. S., Poh, C. L., and Chang, M. W. (2011) Engineering microbes to sense and eradicate Pseudomonas aeruginosa, a human pathogen. *Mol. Syst. Biol. 7*, 521.

(20) Uriu, K. (2016) Genetic oscillators in development. *Dev., Growth Differ. 58*, 16−30.

(21) Windgassen, M., Urban, A., and Jaeger, K.-E. (2000) Rapid gene inactivation in Pseudomonas aeruginosa. *FEMS Microbiol. Lett. 193*, 201−205.

(22) Choi, K. H., and Schweizer, H. P. (2006) mini-Tn7 insertion in bacteria with single attTn7 sites: example Pseudomonas aeruginosa. *Nat. Protoc. 1*, 153−161.

(23) Xia, A., Han, J., Jin, Z., Ni, L., Yang, S., and Jin, F. (2018) Dual-Color Fluorescent Timer Enables Detection of Growth-Arrested Pathogenic Bacterium. *ACS Infect. Dis. 4*, 1666−1670.

(24) Cirz, R. T., O'Neill, B. M., Hammond, J. A., Head, S. R., and Romesberg, F. E. (2006) Defining the Pseudomonas aeruginosa SOS response and its role in the global response to the antibiotic ciprofloxacin. *J. Bacteriol. 188*, 7101−7110.

(25) Michel, B., Sinha, A. K., and Leach, D. R. F. (2018) Replication fork breakage and restart in Escherichia coli. *Microbiol. Mol. Biol. Rev. 82*, e00013−00018.

(26) Bhowmik, B. K., Clevenger, A. L., Zhao, H., and Rybenkov, V. V. (2018) Segregation but not replication of the Pseudomonas aeruginosa chromosome terminates at dif. *mBio 9*, e01088−01018.
(27) Bi, X., and Liu, L. F. (1994) recA-independent and recA-dependent Intramolecular Plasmid Recombination: Differential Homology Requirement and Distance Effect. *J. Mol. Biol. 235*, 414−423.
(28) Smith, G. R. (2012) How RecBCD enzyme and Chi promote DNA break repair and recombination: a molecular biologist's view. *Microbiol. Mol. Biol. Rev. 76*, 217−228.
(29) Dillingham, M. S., and Kowalczykowski, S. C. (2008) RecBCD enzyme and the repair of double-stranded DNA breaks. *Microbiol. Mol. Biol. Rev. 72*, 642−671. Table of Contents.
(30) Morimatsu, K., and Kowalczykowski, S. C. (2003) RecFOR Proteins Load RecA Protein onto Gapped DNA to Accelerate DNA Strand Exchange: A Universal Step of Recombinational Repair. *Mol. Cell 11*, 1337−1347.
(31) Wakamatsu, T., Kitamura, Y., Kotera, Y., Nakagawa, N., Kuramitsu, S., and Masui, R. (2010) Structure of RecJ exonuclease defines its specificity for single-stranded DNA. *J. Biol. Chem. 285*, 9762−9769.
(32) Lovett, S. T., and Clark, A. J. (1984) Genetic analysis of the recJ gene of Escherichia coli K-12. *J. Bacteriol. 157*, 190.
(33) Feschenko, V. V., Rajman, L. A., and Lovett, S. T. (2003) Stabilization of perfect and imperfect tandem repeats by single-strand DNA exonucleases. *Proc. Natl. Acad. Sci. U. S. A. 100*, 1134.
(34) Harmon, F. G., and Kowalczykowski, S. C. (1998) RecQ helicase, in concert with RecA and SSB proteins, initiates and disrupts DNA recombination. *Genes Dev. 12*, 1134−1144.
(35) Lloyd, R. G., and Buckman, C. (1985) Identification and genetic analysis of sbcC mutations in commonly used recBC sbcB strains of Escherichia coli K-12. *J. Bacteriol. 164*, 836.
(36) Kushner, S. R., Nagaishi, H., Templin, A., and Clark, A. J. (1971) Genetic Recombination in Escherichia coli: The Role of Exonuclease I. *Proc. Natl. Acad. Sci. U. S. A. 68*, 824.
(37) Wendel, B. M., Cole, J. M., Courcelle, C. T., and Courcelle, J. (2018) SbcC-SbcD and ExoI process convergent forks to complete chromosome replication. *Proc. Natl. Acad. Sci. U. S. A. 115*, 349−354.
(38) Uranga, L. A., Reyes, E. D., Patidar, P. L., Redman, L. N., and Lusetti, S. L. (2017) The cohesin-like RecN protein stimulates RecA-mediated recombinational repair of DNA double-strand breaks. *Nat. Commun. 8*, 15282.
(39) Worth, L., Clark, S., Radman, M., and Modrich, P. (1994) Mismatch repair proteins MutS and MutL inhibit RecA-catalyzed strand transfer between diverged DNAs. *Proc. Natl. Acad. Sci. U. S. A. 91*, 3238.
(40) Carrasco, B., Serrano, E., Martin-Gonzalez, A., Moreno-Herrero, F., and Alonso, J. C. (2019) Bacillus subtilis MutS Modulates RecA-Mediated DNA Strand Exchange Between Divergent DNA Sequences. *Front. Microbiol. 10*, 237.
(41) Marie, L., Rapisarda, C., Morales, V., Berge, M., Perry, T., Soulet, A. L., Gruget, C., Remaut, H., Fronzes, R., and Polard, P. (2017) Bacterial RadA is a DnaB-type helicase interacting with RecA to promote bidirectional D-loop extension. *Nat. Commun. 8*, 15638.
(42) Torres, R., Serrano, E., and Alonso, J. C. (2019) Bacillus subtilis RecA interacts with and loads RadA/Sms to unwind recombination intermediates during natural chromosomal transformation. *Nucleic Acids Res. 47*, 9198−9215.
(43) Hall, M. C., Jordan, J. R., and Matson, S. W. (1998) Evidence for a physical interaction between the Escherichia coli methyl-directed mismatch repair proteins MutL and UvrD. *EMBO J. 17*, 1535−1541.
(44) Petrova, V., Chen, S. H., Molzberger, E. T., Tomko, E., Chitteni-Pattu, S., Jia, H., Ordabayev, Y., Lohman, T. M., and Cox, M. M. (2015) Active displacement of RecA filaments by UvrD translocase activity. *Nucleic Acids Res. 43*, 4133−4149.
(45) Ahn, B. (2000) A Physical Interaction of UvrD with Nucleotide Excision Repair Protein UvrB. *Mol. Cells 10*, 592−597.
(46) Arthur, H. M., and Lloyd, R. G. (1980) Hyper-recombination in uvrD mutants of Escherichia coli K-12. *Mol. Gen. Genet. 180*, 185−191.
(47) Mehta, A., and Haber, J. E. (2014) Sources of DNA double-strand breaks and models of recombinational DNA repair. *Cold Spring Harbor Perspect. Biol. 6*, a016428.
(48) Lusetti, S. L., and Cox, M. M. (2002) The bacterial RecA protein and the recombinational DNA repair of stalled replication forks. *Annu. Rev. Biochem. 71*, 71−100.
(49) Lovett, S. T. (2017) Template-switching during replication fork repair in bacteria. *DNA Repair 56*, 118−128.
(50) Nowak, M. A. (2006) *Evolutionary dynamics: exploring the equations of life*, Harvard University Press, Cambridge, MA.

https://dx.doi.org/10.1021/acssynbio.9b00256
ACS Synth. Biol. 2020, 9, 1041−1050